*Desalination and Water Treatment*
www.deswater.com

doi: 10.5004/dwt.2018.21946

108 (2018) 27–39
March

# Impact of forming on the structure and separation properties of polyacrylonitrile membranes with polyaniline addition

Beata Fryczkowska*, Dorota Biniaś, Czesław Ślusarczyk, Janusz Fabia, Jarosław Janicki

*Faculty of Materials, Civil and Environmental Engineering, Institute of Textile Engineering and Polymer Materials, University of Bielsko-Biała, Willowa 2, 43-309 Bielsko-Biała, Poland, emails: bfryczkowska@ath.bielsko.pl (B. Fryczkowska), dbinias@ath.bielsko.pl (D. Biniaś), cslusarczyk@ath.bielsko.pl (C. Ślusarczyk), jfabia@ath.bielsko.pl (J. Fabia), jjanicki@ath.bielsko.pl (J. Janicki)*

Received 25 July 2017; Accepted 24 January 2018

**ABSTRACT**

The paper presents the results of research regarding the effects of adding polyaniline (PANI) to polyacrylonitrile (PAN) and the impact of coagulation bath type on the transport and separation properties of composite PAN/PANI membranes. Membranes were obtained by phase inversion from a solution containing PAN:PANI (12:1) dissolved in *N*,*N*-dimethylformamide (DMF). As a result of coagulation in water and/or an aqueous solution of camphorsulphonic acid (CSA), PAN/PANI composite membranes were obtained. It is herein demonstrated that adding non-protonated PANI to the PAN leads to the formation of membranes, whose maximum water flux was approximately 350 L/m$^2$ × h and rejection coefficients were approximately 28% ÷ 51% for $Fe^{3+}$ and 80% for bovine serum albumin (BSA). In contrast, composite membrane that was coagulated in CSA had different properties with a volumetric permeate flux of approximately 152 L/m$^2$ × h and the rejection coefficients of approximately 84% (for $Fe^{3+}$) and approximately 20% (for BSA). Wide-angle X-ray scattering studies, attenuated total reflectance infrared spectroscopy (infrared spectroscopy), differential scanning calorimetry, thermogravimetric analysis and scanning electron microscopy confirmed that the supramolecular structure of composite membranes differs from one to another, which affects its transport and separation properties.

*Keywords:* Polyaniline; Polyacrylonitrile; Composite; Rejection; Morphology; Structure

## 1. Introduction

Polyacrylonitrile (PAN) is a well-known polymer that is widely used in various applications. It is soluble in *N*,*N*-dimethylformamide (DMF), dimethyl sulphoxide (DMSO), dimethylacetamide (DMAc), chloroacetonitrile, dioxanone, dimethyl phosphite, dimethyl sulphone, γ-butyrolactone, ethylene carbonate, nitric acid and sulphuric acid, and it is thus processed from a solution [1,2]. PAN membranes can be obtained using the phase inversion method. Using the appropriate process conditions, such as polymer concentration, solvent type, coagulant type, solvent evaporation time and temperature, non-porous and porous membranes can be obtained [3–6]. These membranes are used in pressure membrane processes such as ultrafiltration (UF), nanofiltration, reverse osmosis, pervaporation and gas separation [4,7–9]. There are many techniques for modifying PAN membranes to give them new properties. PAN can by hydrophilized physically with plasma treatment [7,10], or chemically with treatment by sodium hydroxide [4,9,11–13]. The static tendencies of PAN are sometimes a disadvantage that hampers its use, and an interesting solution is introducing a conductive polymer such as polyaniline (PANI). Addition of PANI to PAN not only allows for the drainage of electrostatic charges that accumulate on the membrane but also reduces the fouling phenomenon [14].

PANI belongs to the group of the most well-known and studied conductive polymers, which also includes

* Corresponding author.

1944-3994/1944-3986 © 2018 Desalination Publications. All rights reserved.

polyacetylene, polypyrrole and polythiophene. PANI is a low-cost polymer that is easy to obtain [15]. It has many advantages, such as good electrical properties and thermal and chemical stability, which enables many opportunities for its application. This polymer is used in batteries, capacitors, and anticorrosion and antistatic coatings [16,17] in the manufacturing of detectors, sensors and biosensors [18–21].

There are many techniques for obtaining PAN membranes with added PANI. Some are based on the classical phase inversion method, and others are based on the preparation of membranes through electrospinning. A simple technique for the preparation of solutions containing both PAN and PANI is the use of a solvent that is common for both polymers. Raeesi et al. [22] prepared two separate solutions in a solvent, *N*-methyl-2-pyrrolidone (NMP), and then mixed them together to obtain a PAN/PANI/NMP solution, which was used for the preparation of nanofibres. Kizildag et al. [23] reported a method of preparing a PAN/PANI solution from DMSO or DMF. First, they prepared a PANI solution that was additionally protonated with camphorsulphonic acid (CSA), dodecylbenzene sulfonic acid (DBSA) or its sodium salt. PAN was introduced to the prepared solutions of protonated PANI in DMSO or DMF to make a solution that was used for the preparation of fibres through electrospinning. Other works describe a technique of obtaining the composite from DBSA-protonated PANI dissolved and mixed with PAN solution in DMSO with a film that is poured and dried at elevated temperature (60°C) [24].

The paper presents the results of research regarding the possibility of doping PAN with the use of a conductive polymer in order to obtain membranes with new, undescribed transport and separation properties. PANI, in its protonated and deprotonated forms, was used as the additive (Fig. 1). Membranes were prepared using the phase inversion method, starting with a homogeneous solution of both polymers in DMF, and through coagulation in water and/or CSA. The concentration of PAN in DMF was 12% because, according to Scharnagl and Buschatz [3], it is the optimum concentration for the preparation of membranes with good separation properties. The choice of CSA was determined from literature that indicates that it is the best acid to use for PANI protonation [25]. In this study, the transport and separation properties of PAN/PANI membranes were analyzed using a $FeCl_3$ solution (with a concentration of 0.1 g/dm$^3$) and a solution of BSA (with a concentration of 1 g/dm$^3$).

Results showed that the PAN/PANI composite membranes were characterized by different properties, depending on the choice of coagulation method used. The composite membranes containing non-protonated PANI were characterized by high values of volumetric permeate flux, low $Fe^{3+}$ ion rejection coefficients and high BSA rejection coefficients. Membranes that contained protonated PANI (membrane C) behaved conversely, with low values of volumetric permeate flux, high iron(III) ions and low BSA rejection coefficients. The different behaviour of membrane C was confirmed from X-ray structure tests (wide-angle X-ray scattering [WAXS]), in which the presence of crystalline areas was demonstrated not only for the PAN but also for the PANI. A full description of PAN/PANI composite membranes was obtained using scanning electron microscopy (SEM), attenuated total reflectance infrared spectroscopy (ATR-IR) and thermal analysis (differential scanning calorimetry [DSC] and thermogravimetric analysis [TGA]).

## 2. Experimental section

### 2.1. Materials

The PAN ($M_w$ = 85.000) copolymer (93.9% acrylonitrile/5.8% methyl acrylate/0.3% methallyl sulphonate) was purchased from GoodFellow Cambridge Ltd. (Cambridge, UK) Polyaniline (PANI) ($M_w$ = 50.000), CSA and bovine serum albumin (BSA; $M_w$ = 66 kDa) were purchased from Sigma-Aldrich (Poznań, Poland). DMF and anhydrous $FeCl_3$ were purchased from Avantor Performance Materials Poland S.A (Gliwice, Poland).

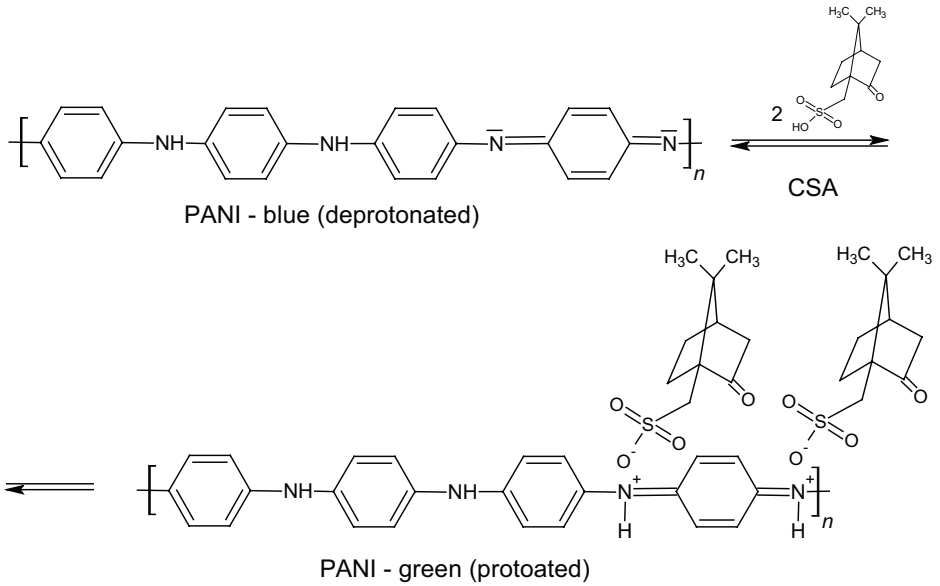


Fig. 1. Chemical structure of polyaniline.

### 2.2. Membrane formation

#### 2.2.1. Formation of PAN membranes

PAN membranes were prepared using phase inversion, and the method for their preparation is described in our previous paper [26].

Initially, a 12% w/w solution in DMF was prepared by dissolving the polymer at room temperature. The PAN solution was then poured onto a glass plate and was spread with a casting knife with an adjustable thickness fixed at 0.2 mm. Finally, it was rapidly coagulated in distilled water at room temperature until the membrane detached from the glass. The precipitated membranes (membrane "0") were air-dried by interposing a layer of tissue paper and applying the load of a glass plate.

#### 2.2.2. Formation of composite PAN/PANI membranes

Composite PAN membranes with PANI addition were prepared using phase inversion, and the method for their preparation is described in our previous paper [26].

Initially, a 1% w/w solution of PANI in DMF was prepared, and then PAN was added to it in an amount such that the concentration of the polymer was 12% w/w. The resulting solution was used to form membranes using the phase inversion method. For this purpose, the polymer solution was poured onto a glass plate and the polymer film was formed using a casting knife with an adjustable thickness fixed at 0.2 mm, which was then coagulated in three different baths at room temperature. The coagulating baths were: (a) water (membrane A); (b) water followed by a 0.1 M solution of CSA for 30 s (membrane B) and (c) a 0.1 M solution of CSA (membrane C). The resulting membranes were air-dried between tissue paper under the load of glass plate.

### 2.3. Physical properties of membranes

The sorption of water ($U$) was measured as follows: dry membrane samples ($W_d$) with dimensions of 1 × 1 cm were weighed on an analytical balance with an accuracy of 0.0001 g and were then immersed in distilled water for 10 s. The membranes were then blotted on filter paper and were weighed again in their wet state ($W_w$). The sorption of water was calculated according to Eq. (1):

$$U = \left( \frac{W_w - W_d}{W_d} \right) \times 100\% \quad (1)$$

The porosity of the membranes (ε), which is defined as the ratio of pore volume to the volume of the membrane, was calculated using Eq. (2):

$$\varepsilon = \left( \frac{(W_w - W_d)/d_w}{(W_w - W_d)/d_w + W_d/d_p} \right) \times 100\% \quad (2)$$

where $d_w$ is the density of distilled water (0.998 g/cm$^3$) and $d_p$ is the polymer density (1.184 g/cm$^3$) [1].

The static contact angle was measured using a goniometer (FIBRO System AB PG-1). Thus, the tests were performed in the skin (top) layer of the membranes.

### 2.4. Characterization techniques

#### 2.4.1. FTIR-ATR spectroscopy

All measurements were carried out using a Fourier transform infrared spectroscopy (FTIR) spectrometer Nicolet 6700 (Thermo Electron Corp., Madison, WI, USA) with an ATR accessory. The ATR accessory had a multiple bounce crystal of KRS (iodobrome thallium-TlBrI) and an angle of incidence of 45°. The following spectrometer parameters were used: resolution 4 cm$^{-1}$, spectral range 500–4,000 cm$^{-1}$, (DTGS) detector and spectra were averaged from 256 scans. Data collection and post-run processing were performed using the OMNIC software (v. 8.0, Thermo Electron Corp., Madison, WI, USA).

#### 2.4.2. X-ray scattering (WAXS)

X-Ray diffraction investigations were performed with a URD 63 Seifert diffractometer. Cu K$\alpha$ radiation was used at 40 kV and 30 mA. Monochromatization of the beam was obtained by means of a nickel filter and a pulse-height analyzer. A scintillation counter was used as a detector. Investigations were performed at a range of angles from 18° to 26° with a step of 0.01°. Each diffraction curve was corrected for polarization, the Lorentz factor and incoherent scattering.

#### 2.4.3. Differential scanning calorimetry

A TA Instruments MDSC 2920 calorimeter was used. Measurements were made in a nitrogen atmosphere (flow 40 mL/min) in the heating mode at a rate of 10 and 60°/min, respectively, in the range of –40°C to 320°C. The obtained DSC curves were analyzed using the TA Instruments Universal V4.5A software package.

#### 2.4.4. Thermogravimetric analysis

TGA investigations were performed using a TA Instruments Q500 Thermogravimetric Analyzer. Measurements were made over a temperature range of 30°C–800°C with a heating rate of 20°/min in a nitrogen atmosphere (flow 40 mL/min). The data were evaluated using the TA Instruments Universal V4.7A software.

#### 2.4.5. Scanning electron microscopy

Membrane surface morphologies and their cross-sections were observed using a JSM 5500 LV JEOL scanning electron microscope. All samples were coated with a layer of gold in a JEOL JFC 1200 vacuum coater at 3 × 10$^{-5}$ Torr.

#### 2.4.6. Measurements of water flux

Transport properties of the obtained membranes were tested using a Millipore's Amicon 8400 UF cell with a capacity of 350 cm$^3$ and a membrane diameter of 7.6 cm that was equipped with equalizing tank with a capacity of 800 cm$^3$.

At the beginning, dry membranes were immersed in distilled water for 1 h. Then, they were treated with distilled water for 2 h under a pressure of 0.2 MPa (which is beneficial for the membrane stability). Tests were performed at a working pressure of 0.1, 0.15 and 0.2 MPa. The permeate flux ($J_v$) was calculated using Eq. (3):

$$J_v = \frac{Q}{A \times t} \tag{3}$$

where $J_v$ is the water flux (L/m² × h), $Q$ is the volume of permeate water (L), $A$ is the effective membrane area (m²) and $t$ is the permeation time (h).

*2.4.7. Measurements of rejection*

Additionally, studies of membrane separation properties were also conducted using an anhydrous $FeCl_3$ aqueous solution with a concentration of 0.1 g/dm³. To this end, the solution of iron ions was inserted into the UF cell with the previously treated membrane. In addition, a mixing element (a magnetic bar) was inserted into the UF cell and the contents were mixed using the magnetic stirrer. The permeation process was performed at a pressure of 0.2 MPa, drawing the permeate every 10 min and measuring the volume. Permeate flux ($J_v$) was calculated using Eq. (3), assuming that in this case, $Q$ is the permeate volume ($FeCl_3$ solution) per unit of time (m³/s). The concentration of $FeCl_3$ solution in the permeate was determined using a Perkin Elmer Lambda 35 UV-Vis spectrophotometer by measuring the absorbance of the solution at a wavelength of 260 nm. Based on the calibration curve, the concentrations of ferric ions in each sample were calculated. Then, Eq. (4) was used to calculate to rejection performance ($R$) for $FeCl_3$:

$$R = \left(1 - \frac{C_p}{C_f}\right) \times 100\% \tag{4}$$

where $R$ is the rejection performance (%), $C_p$ is the permeate concentration and $C_f$ is the feed concentration. The results are presented in Table 3.

In addition, the occurrence of the fouling phenomenon was studied using an aqueous solution of BSA with a concentration of 1 g/dm³ [14]. To do this, 200 cm³ of BSA solution was inserted into the UF cell with the previously treated membrane. In addition, a mixing element (a magnetic bar) was inserted into the UF cell and the contents were mixed using the magnetic stirrer. The permeation process, similar to Tran et al. [7], was performed at a pressure of 0.2 MPa, drawing a permeate every 10 min and measuring the volume. Permeate flux ($J_v$) was calculated using Eq. (3), assuming that in this case, $Q$ is the permeate volume (BSA solution) per unit of time (m³/s). The concentration of BSA solution in the permeate was determined using a Perkin Elmer Lambda 35 UV-Vis spectrophotometer by measuring the absorbance of the solution at a wavelength of 280 nm. Based on the calibration curve, the concentrations of BSA in each sample were calculated. Then, Eq. (4) was used to calculate the BSA rejection performance ($R$).

Pictures of the membranes after the UF of $FeCl_3$ solutions are shown in Fig. 2. The image of membrane C reveals an orange colouration that arises from $Fe^{3+}$ ions, which precipitate on the membrane to form fouling.

## 3. Results and discussion

This paper describes the impact of the type of coagulant used on the physicochemical, transport and separation properties of composite PAN membranes with the addition of PANI. The membranes were prepared using the phase inversion method from a PAN/PANI/DMF solution through coagulation in water and an aqueous solution of CSA. The effects of the addition of PANI on membrane formation and the impact of CSA on the ordering of phases in the polymer composite were analyzed.

### *3.1. Membrane characteristics*

Physicochemical properties such as the contact angle, water sorption and porosity of membranes obtained in the experiment were examined. The tests showed that the membranes obtained from pure PAN are hydrophilic and their

Table 2
The results of studies of volumetric permeate flux for distilled water

| Membrane | $J_v$ (L/m² × h) | | |
|---|---|---|---|
| | 0.1 (MPa) | 0.15 (MPa) | 0.2 (MPa) |
| 0 | 57.96 ± 4.14 | 120.95 ± 10.24 | 195.85 ± 17.61 |
| A | 215.7 ± 10.31 | 289.8 ± 23.20 | 354.38 ± 29.54 |
| B | 128.89 ± 9.90 | 190.82 ± 13.91 | 248.12 ± 20.72 |
| C | 85.22 ± 7.62 | 119.63 ± 8.97 | 151.65 ± 13.59 |

Table 1
Values of characteristic temperatures of the glass transition (determined using the half-height procedure) of amorphous $T_g1$ and mesomorphic $T_g2$ phases and melting $T_m$, evaluated based on DSC curves (Fig. 7) for the investigated PAN membranes

| Membrane | Temperature of glass transition of amorphous phase, $T_g1$ (°C) | Temperature of glass transition of mesomorphic phase, $T_g2$ (°C) | Temperature of melting, $T_m$ (°C) |
|---|---|---|---|
| 0 | 67.0 | 125.9 | 287.0 |
| A | 65.0 | 128.4 | 286.6 |
| B | 68.5 | 217.6 | 267.6 |
| C | 61.3 | 133.0 | 273.5 |

Table 3
Volumetric permeate flux and the rejection of $Fe^{3+}$ ions on the membranes

| Permeation time (min) | Membrane 0 | | Membrane A | | Membrane B | | Membrane C | |
|---|---|---|---|---|---|---|---|---|
| | $J_v$ (L/m² × h) | $R$ (%) | $J_v$ (L/m² × h) | $R$ (%) | $J_v$ (L/m² × h) | $R$ (%) | $J_v$ (L/m² × h) | $R$ (%) |
| 10 | 282.21 ± 12.35 | 44.49 | 339.09 ± 15.61 | 34.23 | 185.76 ± 5.33 | 50.51 | 115.69 ± 3.32 | 83.96 |
| 20 | 236.03 ± 10.07 | 36.41 | 232.52 ± 12.87 | 31.82 | 156.27 ± 4.81 | 43.29 | 93.09 ± 6.56 | 80.73 |
| 30 | 207.70 ± 5.98 | 34.06 | 184.96 ± 9.02 | 30.87 | 126.22 ± 4.95 | 40.88 | 80.99 ± 4.1 | 79.17 |
| 40 | 186.78 ± 6.31 | 32.91 | 153.55 ± 7.96 | 30.11 | 115.83 ± 3.28 | 39.37 | 72.31 ± 4.09 | 77.65 |
| 50 | 170.81 ± 5.50 | 32.28 | 131.26 ± 8.25 | 29.46 | 104.74 ± 4.99 | 38.90 | 65.31 ± 3.89 | 76.89 |
| 60 | 158.31 ± 4.22 | 31.65 | 119.68 ± 7.45 | 28.85 | 96.52 ± 5.23 | 37.86 | 59.55 ± 4.28 | 76.07 |
| 70 | 146.68 ± 9.34 | 31.27 | 107.08 ± 6.99 | 28.69 | 90.32 ± 4.19 | 37.68 | 54.35 ± 3.67 | 75.99 |
| 80 | 145.28 ± 9.25 | 31.02 | 105.12 ± 6.72 | 28.49 | 89.72 ± 5.38 | 37.71 | 54.05 ± 4.53 | 75.23 |

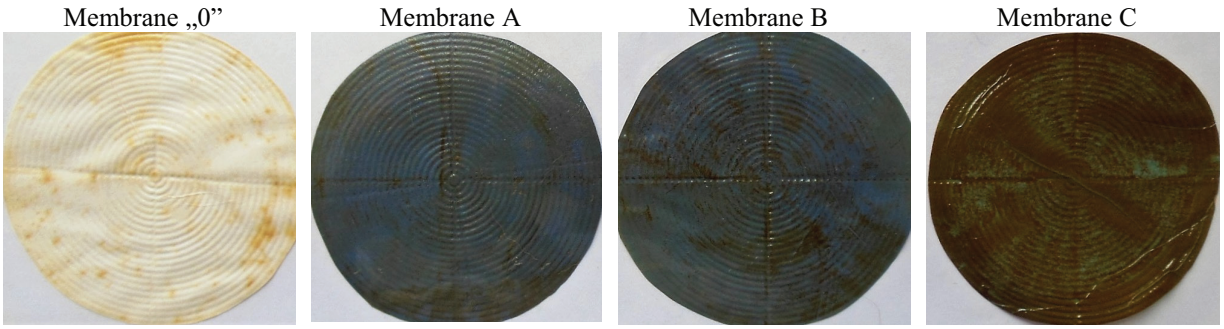


Fig. 2. Surfaces of the membranes after studying the separation properties using a $FeCl_3$ solution.

static contact angle is 13.97° ± 1.27°. For membranes with added PANI, a change in the contact angle was observed depending on the coagulant that was used in the membrane formation process. The use of water for the coagulation of PAN/PANI membranes resulted in a reduction of the contact angle to 11.15° ± 0.91°. In contrast, contact angle of membrane B, which was precipitated from water and then washed with CSA, demonstrated a slightly lower hydrophilicity (11.74° ± 1.23°). For membranes coagulated in CSA, the contact angle was 18.57° ± 2.09°, which is even higher than the result that was obtained for membrane "0."

The conducted research shows that the use of PAN with the addition of PANI influences the hydrophilicity of the polymer matrix. The non-protonated PANI slightly reduces the contact angle. The coagulation process of PAN/PANI membranes in the presence of CSA leads to permanent protonation of the conductive polymer because the acid molecule chemically binds to the PANI to form an amine salt. In addition, the structural composition of CSA, the hydrocarbon fragment of which is hydrophobic, can affect the partial hydrophobization of the composite membrane surface.

Porosity calculations confirmed the high porosities of the composite membranes that were obtained. The porosity of membrane "0" was approximately 80.5%, and slightly lower values were obtained for membranes A (approximately 85.2%) and B (approximately 82.5%). Membrane C had the lowest porosity of all the membranes, which was approximately 69.2%. The results confirm the impact of PANI when it is added to PAN. High porosity values are associated with the hydrophilicity of the composite membranes A and B. In contrast, the more hydrophobic membrane C has lower porosity.

### 3.2. SEM analysis

The analysis of the surface and cross-sections of the membranes using SEM (Fig. 3) allowed us to observe the impact of forming conditions on the external and internal structure, as well as the thickness and porosity of the membranes. The SEM images show that asymmetric membranes are produced in the formation process. The cross-section of membrane "0" (Fig. 3; 0-1) reveals a finger-like structure that is very characteristic of asymmetric membranes that have been described by Ren and McCutcheon [27]. The thickness of the skin for the pure PAN membrane "0" is approximately 0.87 μm. The cross-sections of membranes A and B are similar to each other. For these composite membranes (Fig. 3; A-1, B-1), the thickness of the skin layer is slightly smaller and is approximately 0.82 μm. This results from the addition of PANI, which slows the formation of PAN/PANI membranes. In addition to the low contact angle (11.2°–11.7°), the cross-sectional images confirm the hydrophilic nature of membranes A and B. In Fig. 3 (A-1, B-1), large chambers surrounded by thin but porous walls are visible. Such an arrangement of the cross-section and high porosity (82.5%–85.2%) is observed during the slow coagulation of membranes.

For membrane C (Fig. 3; C-1), a finger-like structure was also observed, but it was partially covered during the sample preparation process. The membrane that was coagulated in CSA is characterized by nearly double the thickness of the skin layer (about 1.5 μm). Analyzing the microphotograph of membrane C, it is apparent that the structure is very porous, both at the macro- and micro-scale. The observed structure is also more compact than the others, resulting in

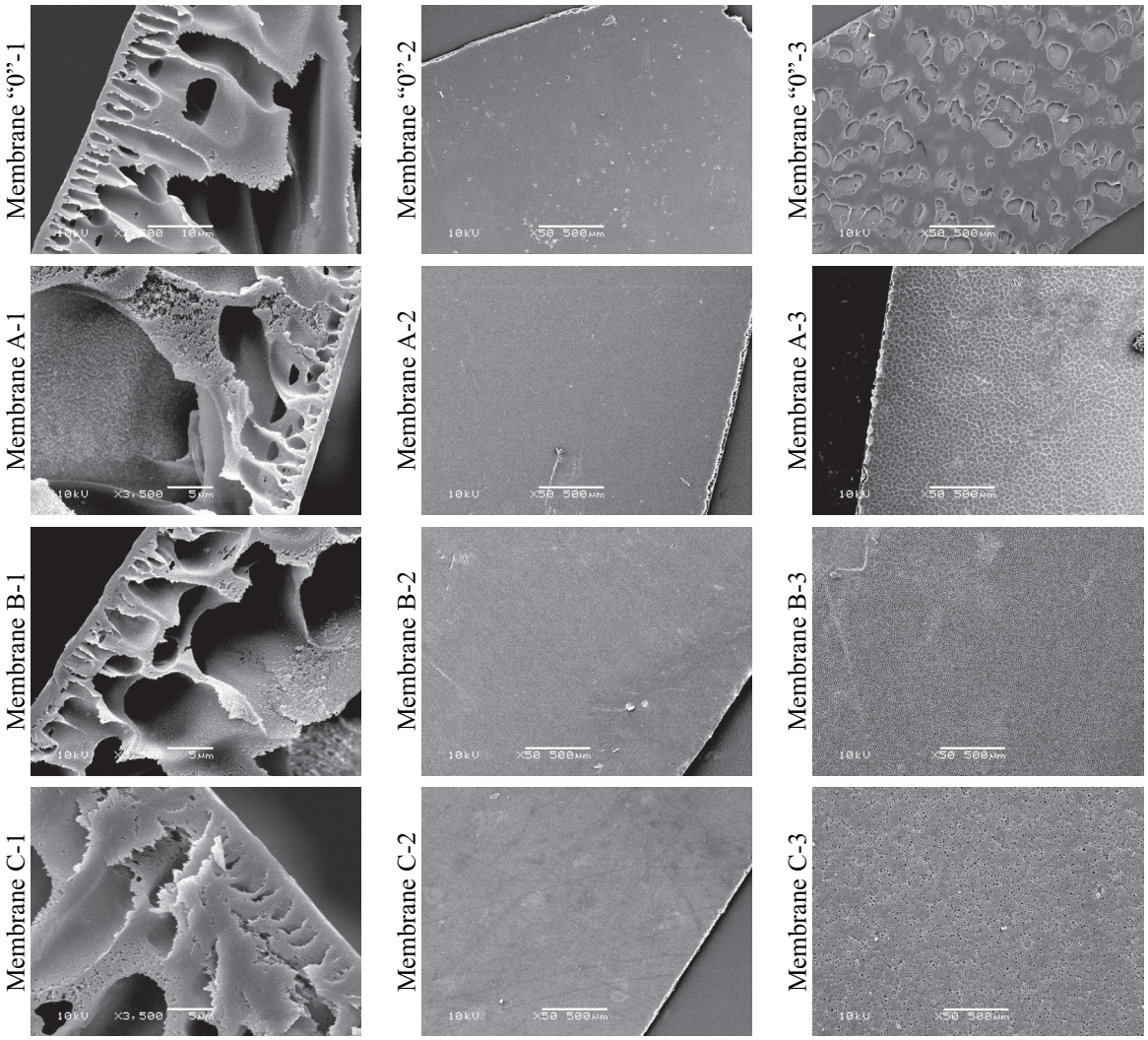


Fig. 3. Microphotographs (SEM) of pure PAN ("0") and PAN/PANI composite membranes (A–C): (1) cross-section, (2) skin layer and (3) bottom layer.

a porosity of approximately 69%. The structure of the membrane cross-section (Fig. 3; C-1) may indicate that the coagulation process occurred more rapidly than in other membranes.

The SEM images of the skin layer of all examined composite membranes (Fig. 3. "0"-2; A-2; B-2; C-2) show a smooth structure with no visible pores. The microphotographs of the support layer of the membranes (Fig. 3. "0"-3; A-3; B-3; C-3) are very different. The surface of the support layer of pure PAN membrane (membrane "0") has large and numerous porous openings. The PAN/PANI composite membranes have a structure made of small, shallow hollows. For membrane C (Fig. 3; C-3), small, deep hollows on the surface of the support layer can be observed.

### *3.3. X-ray analysis*

X-ray methods are techniques that allow us to analyze the possibility of occurrence and degree of ordering of polymer chains within the matrix. Fig. 4(a) shows the curves of WAXS for membranes in which water was used for coagulation. The curves for PAN/PANI membranes are almost the same as for pure PAN membranes (membrane "0"). The dominant diffraction effect on these curves is a peak, with an angular position of $2\theta \approx 17°$. Its presence indicates the arrangement of PAN chains, with a clear inflexion for membranes A and B, indicating that the peak is a double peak. Such double peaks are characteristic of a paracrystalline arrangement of PAN chains in two dimensions, in a rhombic system with unit cell dimensions of $a = 1.03$ nm and $b = 0.61$ nm [28]. The peaks that are visible on the curves correspond to the diffraction peaks from the (110) and (200) planes, respectively. This confirms a lack of ordering of PAN chains along their axes. Studies also show that for the membranes coagulated in water the PANI chains are not arranged, even if the membrane was immersed in CSA after the coagulation (e.g., membrane B).

Fig. 4(b) shows WAXS curves for the membrane that was coagulated in water only (membrane A) and in the CSA solution only (membrane C). On both curves, a double diffraction peak that is characteristic of the paracrystalline arrangement of the PAN chain is visible. The diffraction

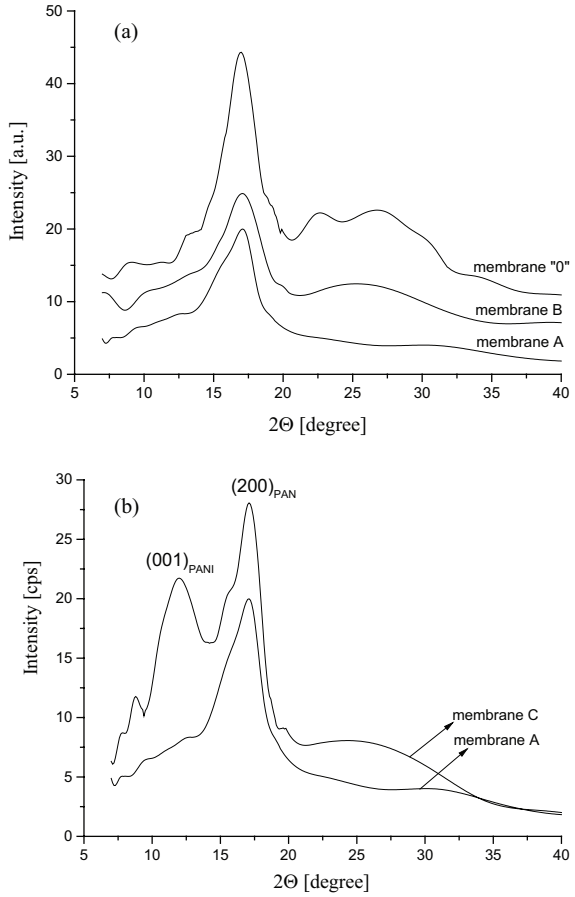


Fig. 4. The WAXS curves for the composite PAN/PANI membranes (A, B, C) and pure PAN membranes ("0").

pattern of sample C shows an additional, strong diffraction peak that is attributed to the arrangement of protonated PANI chains. According to the Łużny model [29], the peak corresponds to diffraction from the (001) plane for the unit cell of the triclinic system that belongs to the *P*1 space group. Analysis of the half-width of the peak enabled us to estimate the size of the areas of the structured PANI chains, for which membrane C is 2.4 nm.

### *3.4. Spectroscopic analysis*

The molecular structure of the skin surface of the membranes was tested using the FTIR spectroscopy ATR method (Fig. 5(a)). In the spectra, characteristic absorption bands in the PAN were observed at 2,925, 2,930, 2,941 and 2,949 $cm^{-1}$ of C–H oscillators stretching vibrations. The bands 1,452 and 1,453 $cm^{-1}$ as well as 1,361 and 1,367 $cm^{-1}$ are attributed to deformation vibrations of C–H oscillators in $CH_2$ units. Stretching vibrations of the nitrile C≡N group occur at a wavenumber of 2,242 and 2,243 $cm^{-1}$ [30]. Bands at 1,730, 1,731, 1,734 and 1,737 $cm^{-1}$ that appear in the spectra are characteristic of stretching vibrations of the C=O oscillator in the ester units (Fig. 5(b)). The spectra obtained for membranes are the result of the presence of approximately 6% of ester comonomers in PAN. For membranes B and C, the band is slightly expanded, which may reveal the additional effect of C=O groups that

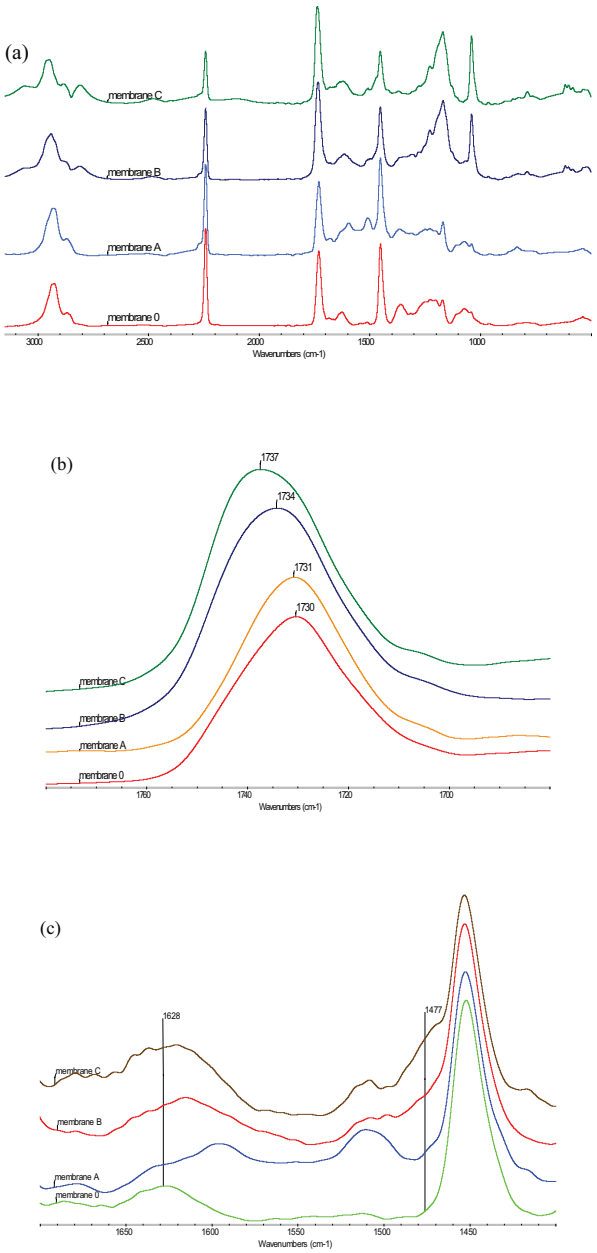


Fig. 5. ATR-FTIR spectra of the composite PAN/PANI membranes (A, B, C) and the pure PAN membrane ("0").

were derived from CSA [31,32]. In the spectra of membranes B and C, there is a band at approximately 1,041 $cm^{-1}$ that is associated with vibrations of the ($SO_3^-$) group [23] that is included in the CSA. This bandwidth is also typical for the effects of $NH^+ \cdots SO_3^-$ groups, resulting from the effects of PANI and CSA [33]. The intensity of this band is higher for membrane C, which was coagulated in a CSA solution [31,32]. The ~1,170 $cm^{-1}$ band that appears in the spectra is due to stretching vibrations of the S=O oscillator in sulphonic acid [23]. This band is visible for membrane "0," which was obtained from the PAN copolymer, containing 0.3% of methallyl sulphonate and is present in the spectrum obtained for membrane A. The band increases in its intensity and width in the spectra of membranes B and C, which confirms the presence of CSA.

Analysis of the bands in the spectra of the membranes A, B and C (Fig. 5(c)) showed insignificant band intensities at ~1,628 and ~1,477 $cm^{-1}$, which are attributed to the stretching vibrations of C=C in the quinone and benzene rings [30]. It can be assumed that PANI is present in minor amounts on the surface of the skin of composite membranes.

### 3.5. DSC analysis

Fig. 6 summarizes the DSC thermograms for samples of pure PAN membrane (membrane "0") recorded during heating at significantly differing rates. On the curve that corresponds to a rate of 10°/min, which is most common in conventional DSC measurements, only the beginning of the process of PAN thermal decomposition is clearly illustrated, in which the first step consists of the cyclization of the polymer chains. Furthermore, in the temperature range of 60°C–120°C on the same DSC curve, there is a disruption of the calorimeter signal line which, based on the analysis of the literature [32,33], should be associated with the glass transition within the disordered PAN phase. However, the low intensity of the effect makes it practically impossible to interpret more completely. With a significant increase (up to 60°/min) of the temperature as a function of measurement time (up to 60°/min), not only are complex thermal effects in terms of glass transition temperatures reflected on the curves, but there is also a pronounced melting peak of paracrystalline PAN phase [34,35] that precedes the onset of polymer thermal decomposition. The abovementioned thermal effects (shown in curve 6 as $T_g1$ and $T_g2$, respectively) are of relaxation nature, which was confirmed by DMA studies [34]. The occurrence of these effects is directly linked to the thermodynamic state transition from glassy to viscoelastic, within the amorphous and mesomorphic PAN phase, which exhibit a type of ordering that are referred to as glass-rubber and glass laterally ordered [34].

For membranes examined in this study, the first of the abovementioned transitions is located in the temperature range 61°C–67°C (Fig. 7; Table 1) and the temperature shift of its characteristic $T_g1$ value does not show a clear changing trends, both for membrane modification using PANI and method of coagulation. However, it should be noted that a very distinct temperature shift of the discussed transformation (approximately 30°C down) for all test membranes with respect to data in the literature was obtained with the DMA method [34]. This phenomenon is likely due to the presence of water, which is difficult to remove from the porous material (membrane), and by forming hydrogen bonds with nitrile groups, relaxes the intermolecular bonds between the PAN chains and consequently causes polymer plasticizing [36]. So-called kinetic segments in the main polymer chain, which are responsible for the glass transition phenomenon, may then be formed at a correspondingly lower temperature.

The second of the abovementioned relaxation changes for the test membranes is observed in the temperature range of 126°C–133°C (Fig. 7; Table 1). Our results, therefore, do not confirm the reports of Pan et al. [24], according to which the addition of PANI causes a slight reduction in the glass transition temperature $T_g2$. In our study, exactly the opposite was observed. By consistently analyzing the DSC curves that were recorded in order of increasing temperature, we finally noticed the effect of melting the paracrystalline mesomorphic phase of PAN (no ordering parallel to the axis of the chain) which, for membranes coagulated with CSA, moves quite clearly towards lower temperatures (for membrane B – almost by as much as 20°C) relative to the unmodified PAN membrane. Considering this, we believe that the presence of the CSA increases the mobility of PAN chains within the paracrystalline phase to move between one another. At the same time, for both membranes, the coincidence of temperature ranges for the melting transition and for the start of thermal decomposition (i.e., cyclization of PAN chains) would confirm the adopted inference.

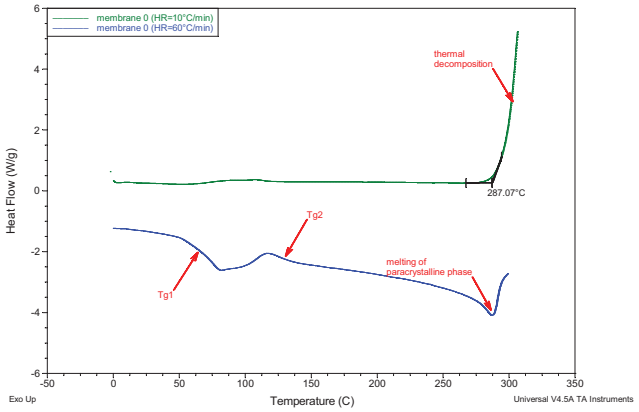


Fig. 6. DSC curves for the unmodified PAN membrane during heating in a nitrogen atmosphere at a rate of 10°C/min (green) and 60°C/min (blue).

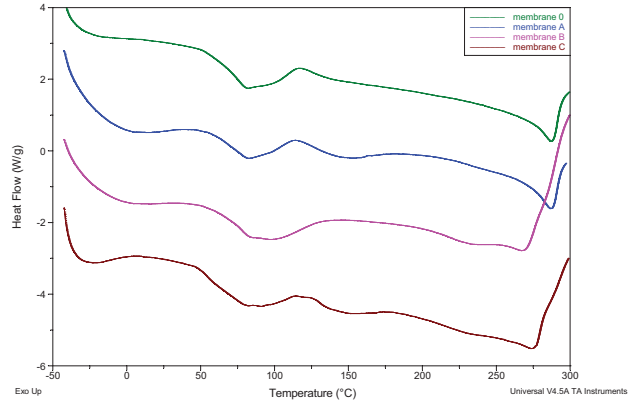


Fig. 7. DSC curves for the investigated membranes obtained from: unmodified PAN (green), and PAN modified with PANI that was precipitated in water (blue), precipitated in water and rinsed in CSA solution (pink) and precipitated in CSA solution (maroon). Curves are registered for a heating rate of 60°C/min in temperature ranges of glass transitions (of amorphous and mesomorphic phases), melting and the beginning of thermal decomposition, respectively.

### 3.6. TGA analysis

In this study, TGA studies of membranes were performed both to determine their thermal stability, as well as to demonstrate the impact of the modifiers that were used (PANI, CSA) on the thermal decomposition of the PAN

matrix. Studies of the thermal stability of PAN composites with added PANI were previously conducted by Al-Ahmed et al. [37]. Fig. 8 summarizes the weight loss curves of the thermogravimetric (TG) and derivative thermogravimetric (dTG) differential curves registered for all the membranes discussed in this paper. The analysis of the curves confirms the full thermal stability of the system, as indicated by Al-Ahmed et al. [37], up to a temperature of approximately 220°C. An exception is membrane A, which loses less than 3% of its mass in the specified temperature range (up to approximately 158°C). Membrane A is a composite membrane that shows the most hydrophilic properties of all membranes that were investigated. Hence, the indicated loss of mass, as also confirmed by Kumar et al. [38], should be connected directly to dehydration of the sample during TGA measurement. Analyzing these TG curves in order of increasing temperature, a few percentage of weight loss is noted for membranes that contain CSA, whose thermal stability is estimated at 198°C. Further, the TG curves for all membranes show a substantial weight loss associated with the thermal dissociation of PAN. This process occurs in two stages (in the case of membrane B, in multiple stages), wherein the stages are not completely separated temperature-wise (i.e., the dTG signal between them is not 0). For the first stage of decomposition, the largest rate of mass loss occurs in the temperature range of 339°C (membrane A) to 350°C (membrane C). In this stage, membrane "0" is characterized by the greatest weight loss (26.4%), whereas membrane A coagulated in water had the lowest (approximately 21%). All membranes that contained PANI in the temperature range show less weight loss compared with the unmodified PAN membrane. In the second stage of thermal dissociation of PAN, the highest rate of weight loss was observed in a much narrower temperature range from 436°C (membrane A) to 440°C (membranes "0" and C). This decomposition stage ends at a temperature of approximately 515°C, and overlaps in its range with the temperature range of the PANI decomposition process that occurs in parallel, as observed by Zhai et al. [39]. At the final temperature of the TGA measurements in the nitrogen atmosphere (less than 800°C), residues of the membrane samples (carbonization products) remained close to half of their initial weights (45.5% and 48.5% for membrane C and membrane 0, respectively).

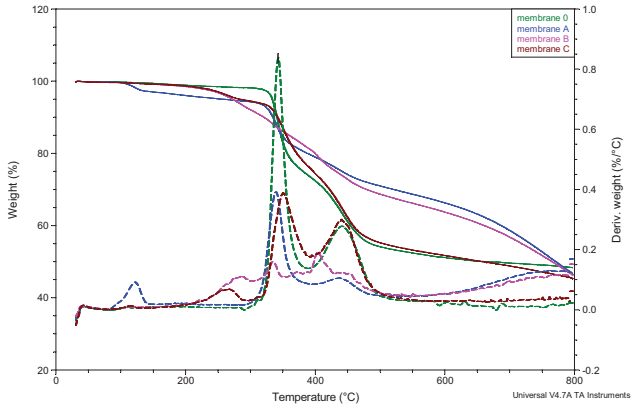


Fig. 8. TG and dTG curves for the investigated membranes.

*3.7. Characterization of membrane permeation*

Transport properties of pure PAN membranes and composite PAN/PANI membranes were characterized by volumetric permeate flux (Table 2).

The volumetric permeate flux (Table 2) for membrane "0" that was obtained from pure PAN assumes values ~58, 121 and 196 L/m$^2$ × h for the pressure values 0.1, 0.15 and 0.2 MPa, respectively. The membrane "0" that was obtained in the experiment was characterized by approximately double the permeate flux at the transmembrane pressure of 0.1 MPa compared with other data given by Tran et al. [7]. The results of earlier studies and observations [26] indicate that the addition of PANI to PAN may hydrophilize the membrane [14], increasing the specific permeate flux value. The study shows that the transport properties of membrane A are four times higher for a pressure of 0.1 MPa, 2.5 times higher for a pressure 0.15 MPa and more than 1.5 times higher for a pressure 0.2 MPa. The membrane flux rate is influenced by its structure and in particular by the morphology of the skin layer. In Fig. 3; A-1, the compact and thin skin that is characteristic of membranes with very good transport properties is observed. In addition, membrane A has the highest porosity (85.2%) and the highest hydrophilicity (11.2°).

A lower value of volumetric permeate flux (water flux) is observed for membrane B, although it is still higher than the value for membrane "0." The observed phenomenon may be the result of the presence of CSA in the membrane, which slightly protonates PANI and slows down the water flux through the membrane. For membrane C, on the other hand, the volumetric permeate flux has the lowest value of all composite membranes, and for a working pressure of 0.2 MPa, the transport properties of this membrane are inferior to the membranes that lack additions. This result may be due to the hydrophobizing of the membrane under the influence of CSA, as described in our previous publication [26]. Membrane C also has the highest contact angle value (18.6°). However, the greatest impact on the transport of liquid through the membranes is the skin layer structure. In the SEM images (Fig. 3; C-1), membrane C has the most compact structure and the skin layer is the thickest (approximately 1.5 μm).

Analysis of the results for the membranes indicate that the addition of PANI improves the transport properties, which are closely related to the membrane porosity and pore interconnection, as described by Fan et al. [14] and Zhao et al. [40]. In summary, we conclude that all the membranes obtained in the experiment exhibit high specific permeate flux values, and the highest values are displayed by the membranes with added PANI (membranes A and B).

Another aspect of the composite membrane studies was determining how the PANI addition impacts the separation of trivalent ferric ions. For this purpose, a feed ($FeCl_3$ solution) was applied to individual membranes and the volumetric permeate flux and $Fe^{3+}$ ion rejection were studied (Table 3).

Fig. 9 shows that the permeate, passing through membrane "0" at the initial stage of the process, improves the membrane properties by approximately 44% (compared with the permeate flux for clean water), followed by a quick decrease to 50% of the initial value. This phenomenon can be explained by the adsorption of a certain amount of iron(III)

ions onto membrane "0," which is accompanied by the formation of "channels" that facilitate the transport of water. This behaviour of membranes has been described in our earlier studies [41]. The rejection of iron(III) ions by membrane "0" is low and decreases during the permeation process from approximately 45% to approximately 31%. This behaviour of the membrane correlates with the size of its pores which retain iron(III) ions ($r_m \approx 0.069 \div 0.078$ nm) to a very low degree (Fig. 2). For membrane A, the initial value of the volumetric permeate flux is similar to the one for distilled water, and then, at the end of the permeation process, it decreases to 32%. These results may indicate the adsorption of polyvalent metal ions on PANI, as described by Ren et al. [42]. Rejection by the membrane is 29%, which is slightly lower than the membrane without additions. Based on the results, it can be assumed that the addition of PANI in a non-protonated form may be present directly on the membrane surface or in open pores. This arrangement of PANI improves the hydrophilic properties of the membrane and makes it easier to "capture" a certain number of trivalent ions. This phenomenon slows the permeate flow through the membrane without retaining iron(III) ions in the pores.

During the formation of membranes B and C, CSA was used for PANI protonation and a schematic of this process is shown in Fig. 1. For membrane B, CSA was used after coagulation of the membrane and membrane C was obtained through precipitation in an aqueous CSA solution. There is similarity in the curves of volumetric permeate flux for membranes B and C. After 10 min of operation, the permeate flux ($FeCl_3$) is reduced by 25%, and by 75% at the end of the measurement for both membranes (A and B). Rejection, on the other hand, is approximately 37% for membrane B, which may be indicative of rinsing the CSA, weakly linked to PANI, and thus the membrane hydrophilization. These interpretations are confirmed by the colour of the membrane (derived from PANI), which after the $FeCl_3$ permeation process changed to blue, which indicates that PANI was deprotonated (Fig. 2). For membrane C, which was coagulated in a CSA solution, a relatively high (compared with the others) rejection value of 76% was observed. This result may indicate that during the coagulation of the PAN/PANI membrane in CSA, the protonation of PANI and precipitation of the polymer occurs in parallel. Protonated PANI is permanently attached to the membrane polymer matrix, resulting in its poor hydrophobization, as described in our previous publication [26]. Thus, membrane C does not form ion "channels" that facilitate the transport of $Fe^{3+}$ to the other side of the membrane, and rather retains them in the form of fouling (Fig. 2). This hypothesis is confirmed by the green colour of the membrane that can be observed in Fig. 2, which indicates that after the permeation process, the PANI remained protonated.

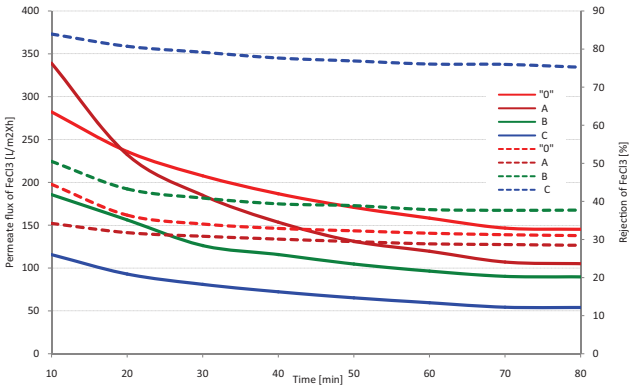


Fig. 9. Volumetric permeate flux (continuous line) and the rejection value (dashed line) of $FeCl_3$.

In summary, we conclude that the addition of PANI in the PAN matrix increases the hydrophilicity of the membrane and prevents the occurrence of fouling [28]. During this study, it was possible to observe the adsorption of a small amount of iron(III) ions on PANI, which did not increase the rejection value. On the other hand, membrane C (which contain protonated PANI), in contrast to other membranes, exhibited hydrophobic properties that resulted in a high rejection value. Unfortunately, a comparison of the results of this study with other works is very difficult because no similar studies have been reported in the literature.

The method that allows us to study the phenomenon of fouling is permeation using organic macromolecular compounds (i.e., proteins such as BSA) [14]. For this purpose, a BSA aqueous solution with a concentration of 1 g/dm$^3$ was prepared and then applied to the membranes for studying the feed transport through the membranes and their rejection factors (Table 4).

Fig. 10 shows that the volumetric permeate flux decreases during operation for all obtained membranes. The greatest decrease was observed for membrane "0," which amounted to 91% within 10 min of the membrane operation.

Table 4
Volumetric permeate flux and the rejection of BSA on the membranes

| Permeation time (min) | Membrane 0 | | Membrane A | | Membrane B | | Membrane C | |
|---|---|---|---|---|---|---|---|---|
| | $J_v$ (L/m$^2$ × h) | $R$ (%) | $J_v$ (L/m$^2$ × h) | $R$ (%) | $J_v$ (L/m$^2$ × h) | $R$ (%) | $J_v$ (L/m$^2$ × h) | $R$ (%) |
| 10 | 29.87 ± 3.03 | 33.40 | 204.63 ± 6.57 | 21.38 | 247.64 ± 8.90 | 60.63 | 147.65 ± 5.02 | 13.90 |
| 20 | 26.79 ± 2.22 | 44.75 | 88.81 ± 4.17 | 24.63 | 126.47 ± 4.50 | 71.61 | 98.49 ± 4.77 | 14.09 |
| 30 | 24.95 ± 1.99 | 57.61 | 52.51 ± 4.25 | 28.80 | 73.82 ± 3.51 | 75.93 | 74.48 ± 5.50 | 15.16 |
| 40 | 24.46 ± 1.96 | 66.90 | 38.50 ± 3.16 | 34.51 | 29.17 ± 1.39 | 76.63 | 69.29 ± 5.01 | 15.17 |
| 50 | 21.57 ± 2.05 | 76.72 | 27.86 ± 3.01 | 47.67 | 17.86 ± 1.13 | 77.40 | 65.53 ± 3.50 | 15.64 |
| 60 | 19.21 ± 1.67 | 78.96 | 22.80 ± 2.98 | 73.78 | 11.20 ± 1.02 | 78.04 | 61.82 ± 3.21 | 18.25 |
| 70 | 18.98 ± 1.94 | 79.04 | 21.36 ± 2.54 | 77.39 | 8.54 ± 1.03 | 78.95 | 59.43 ± 3.56 | 18.77 |
| 80 | 18.29 ± 1.56 | 79.59 | 20.88 ± 1.98 | 79.09 | 5.88 ± 0.54 | 79.08 | 53.32 ± 3.85 | 19.41 |

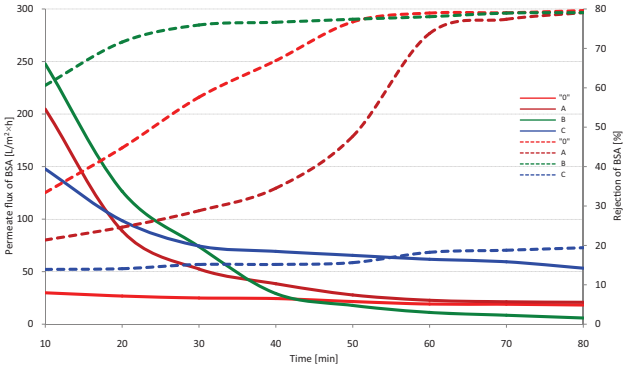


Fig. 10. Specific permeate flux (continuous line) and rejection (dashed line) of BSA.

This observed phenomenon is probably related to the emergence of electrostatic interactions between the negatively charged membrane with PAN and negatively charged BSA molecules. As a result of these interactions, protein fouling on membrane "0" was observed [43,44]. For membrane A, with a PANI addition, the initial decrease in the value of the specific permeate flux for BSA was 42%, and then decreased to a value of approximately 21 L/m$^2$ × h. Lower values of the decrease in the flux through these membranes resulted from the presence of PANI in the PAN matrix. The presence of the conductive polymer leads to a partial discharge of the charges that accumulated on the surface of the membrane, and consequently to slower fouling. Analysis of the results suggests that the hydrophilic membranes from pure PAN (membrane "0") and with the addition of PANI (membrane A) retained large polar molecules of BSA on its surface. Rejection of membrane "0" initially assumes small values (approximately 33%) which then increases rapidly, and after 60 min of the membrane operation, reaches a value of approximately 80%. For membrane A, the rejection initially reaches small values (21%), and after 60 min of operation reaches 80%.

Composite membranes B and C behaved otherwise in the presence of BSA, with initial permeate flux values that were very close to the values for the pure water. Membrane B, after 70 min of operation, was characterized by the worst transport properties (approximately 6 L/m$^2$ × h) and high rejection of about 80%. The value of permeate flux for membrane C fell to approximately 53 L/m$^2$ × h with a low rejection of approximately 19%. These results may be explained by the way in which composite membranes coagulate. Membrane B was coagulated in water and then rinsed with a CSA solution, resulting in the surface protonation of PANI, which disappears during permeate flow, causing slow membrane hydrophilization and retention of BSA particles on the surface. Membrane C, on the other hand, was coagulated in a CSA solution, which resulted in the permanent protonation of PANI that causes membrane C to retain little BSA on the surface, slowly transporting the test solution towards the permeate. In addition, WAXS studies (Fig. 4) have shown that the supramolecular structure of membrane C is different from the other membranes. The analysis of diffraction patterns shows that there are ordered areas not only for the PAN in membrane C but also for the PANI. Therefore, it is highly likely that in protonating PANI, CSA constitutes a major steric hindrance which affects the PANI ordering in the outer layers of membrane C. Chemically, CSA is made of a large aliphatic cycle, which can also affect membrane hydrophobization (Fig. 1). Under these conditions, it is likely that the BSA globules are developed and filtered through membrane C, as observed in this study.

In summary, the conducted tests of separation properties allow us to conclude that the membranes "0," A and B display high rejection of 80%, similarly to Tran et al. [7]. The outcome results from the repulsion of negatively charged particles of PAN membranes and negatively charged BSA particles [43,45]. Membrane C behaves differently compared with the others, which supports its hydrophobic properties. The results may confirm a specific way of ordering of the composite components in the PAN matrix and permanently binding PANI to CSA. The values of the rejection coefficient for membrane C are at the level of values obtained for the poly(ethylene-co-vinyl alcohol) membranes, as described by Hashino et al. [46].

## 4. Conclusions

This paper presents the results of research regarding the effects of adding PANI to PAN membranes and the impact of coagulation bath type on the transport and separation properties of composite PAN/PANI membranes. The membranes were obtained by the phase inversion method from a solution containing both polymers dissolved in DMF, followed by coagulation in water and/or an aqueous solution of CSA.

Composite membrane A, which was coagulated in water, had the highest volumetric permeate flux values of about 350 L/m$^2$ × h (for a pressure of 0.2 MPa). This result demonstrated the hydrophilic properties of this membrane, which was confirmed by the studies of the contact angle, which was 11.15°. The separation of iron(III) ions on membrane A showed a decrease in the permeate flux to approximately 107 L/m$^2$ × h with a rejection coefficient of approximately 29%. BSA separation tests also revealed an unfavourable phenomenon of fouling, and the rejection coefficient of these proteins on membrane A was close to 80%. Similar results were obtained for membrane B, for which the contact angle was 11.74°, the pure water flux was approximately 250 L/m$^2$ × h, and the rejection coefficient was approximately 38% (for $Fe^{3+}$) and approximately 79% (for BSA).

Completely different physicochemical properties were characteristic of the PAN/PANI composite membrane, which was coagulated in CSA. Coagulation in CSA resulted in the formation of ordered PANI areas, as demonstrated by WAXS studies, and the creation of a surface with a higher contact angle of 18.57°. This resulted in a decrease in water flux through membrane C, which was approximately 152 L/m$^2$ × h, the lowest of all membranes. The consequences of this structure were the different separation properties of membrane C. This membrane was characterized by a low volumetric permeate flux (approximately 56 L/m$^2$ × h) and a high rejection coefficient (approximately 76%) for a solution containing $FeCl_3$. On the other hand, the separation of BSA yielded surprisingly good results because the hydrophobic composite membrane C interacts with protein molecules, which are stretched during permeation, from which the fouling occurs in a residual form ($R$ ~ 20%).

SEM analyses confirmed the asymmetric structure of all PAN/PANI composite membranes, which were characterized by a different morphology of the structure and the thickness of the skin layer depending on the method of coagulation. ATR-IR studies confirmed the presence of PAN on the surface of composite membranes, which, in the case of membranes B and C, have additional bands that are characteristic of CSA. Thermal analyses (DSC and TGA) demonstrated that the addition of PANI to the PAN matrix improves and stabilizes the thermal properties of the resulting composites.

## References


[1] G. Wypych, Handbook of Polymers, 2nd ed., ChemTec Publishing, Ontario, Canada, 2016, pp. 271–275.
[2] M.M. Iovleva, V.N. Smirnova, G.A. Budnitskii, The solubility of polyacrylonitrile, Fibre Chem., 33 (2001) 262–264.
[3] N. Scharnagl, H. Buschatz, Polyacrylonitrile (PAN) membranes for ultra- and microfiltration, Desalination, 139 (2001) 191–198.
[4] I.-C. Kim, H.-G. Yun, K.-H. Lee, Preparation of asymmetric polyacrylonitrile membrane with small pore size by phase inversion and post-treatment process, J. Membr. Sci., 199 (2002) 75–84.
[5] H. Lohokare, Y. Bhole, S. Taralkar, U. Kharul, Poly(acrylonitrile) based ultrafiltration membranes: optimization of preparation parameters, Desalination, 282 (2011) 46–53.
[6] P. Wang, Z. Wang, Z. Wu, Insights into the effect of preparation variables on morphology and performance of polyacrylonitrile membranes using Plackett–Burman design experiments, Chem. Eng. J., 193–194 (2012) 50–58.
[7] T.D. Tran, S. Mori, M. Suzuki, Plasma modification of polyacrylonitrile ultrafiltration membrane, Thin Solid Films, 515 (2007) 4148–4152.
[8] K. Nouzaki, M. Nagata, J. Arai, Y. Idemoto, N. Koura, H. Yanagishita, H. Negishi, D. Kitamoto, T. Ikegami, K. Haraya, Preparation of polyacrylonitrile ultrafiltration membranes for wastewater treatment, Desalination, 144 (2002) 53–59.
[9] H.-A. Tsai, Y.-L. Ye, K.-R. Lee, S.-H. Huang, M.-C. Suen, J.-Y. Lai, Characterization and pervaporation dehydration of heat-treatment PAN hollow fiber membranes, J. Membr. Sci., 368 (2011) 254–263.
[10] D. Pal, S. Neogi, S. De, Surface modification of polyacrylonitrile co-polymer membranes using pulsed direct current nitrogen plasma, Thin Solid Films, 597 (2015) 171–182.
[11] T. Wang, J. Lu, L. Mao, Z. Wang, Electric field assisted layer-by-layer assembly of graphene oxide containing nanofiltration membrane, J. Membr. Sci., 515 (2016) 125–133.
[12] W.-S. Hung, Q.-F. An, M. De Guzman, H.-Y. Lin, S.-H. Huang, W.-R. Liu, C.-C. Hu, K.-R. Lee, J.-Y. Lai, Pressure-assisted self-assembly technique for fabricating composite membranes consisting of highly ordered selective laminate layers of amphiphilic graphene oxide, Carbon, 68 (2014) 670–677.
[13] C.-L. Lai, W.-C. Chao, W.-S. Hung, Q. An, M. De Guzman, C.-C. Hu, K.-R. Lee, Physicochemical effects of hydrolyzed asymmetric polyacrylonitrile membrane microstructure on dehydrating butanol, J. Membr. Sci., 490 (2015) 275–281.
[14] Z. Fan, Z. Wang, N. Sun, J. Wang, S. Wang, Performance improvement of polysulfone ultrafiltration membrane by blending with polyaniline nanofibers, J. Membr. Sci., 320 (2008) 363–371.
[15] B.-H. Lee, H.-J. Kim, H.-S. Yang, Polymerization of aniline on bacterial cellulose and characterization of bacterial cellulose/polyaniline nanocomposite films, Curr. Appl. Phys., 12 (2012) 75–80.
[16] S. Vulpe, F. Nastase, C. Nastase, I. Stamatin, PAN–PAni nanocomposites obtained in thermocentrifugal fields, Thin Solid Films, 495 (2006) 113–117.
[17] G. Ciric-Marjanovic, Recent advances in polyaniline research: polymerization mechanisms, structural aspects, properties and applications, Synth. Met., 177 (2013) 1–47.
[18] S. Bhadra, D. Khastgir, N.K. Singha, J.H. Lee, Progress in preparation, processing and applications of polyaniline, Prog. Polym. Sci., 34 (2009) 783–810.
[19] Z.M. Tahir, E.C. Alocilja, D.L. Grooms, Polyaniline synthesis and its biosensor application, Biosens. Bioelectron., 20 (2005) 1690–1695.
[20] B. Adhikari, S. Majumdar, Polymers in sensor applications, Prog. Polym. Sci., 29 (2004) 699–766.
[21] S. Nambiar, J.T.W. Yeow, Conductive polymer-based sensors for biomedical applications, Biosens. Bioelectron., 26 (2011) 1825–1832.
[22] F. Raeesi, M. Nouri, A.K. Haghi, Electrospinning nanofibers of polyaniline-polyacrylonitrile blend nanofibers, e-Polymers, 114 (2009) 1–13.
[23] N. Kizildag, N. Ucar, A. Onen, I. Karacan, Polyacrylonitrile/polyaniline composite nanofiber webs with electrostatic discharge properties, J. Compos. Mater., 50 (2016) 3981–3994.
[24] W. Pan, S.L. Yang, G. Li, J.M. Jiang, Electrical and structural analysis of conductive polyaniline/polyacrylonitrile composites, Eur. Polym. J., 41 (2005) 2127–2133.
[25] A.G. MacDiarmid, A.J. Epstein, Secondary doping in polyaniline, Synth. Met., 69 (1995) 85–92.
[26] B. Fryczkowska, Z. Piprek, M. Sieradzka, R. Fryczkowski, J.B. Janicki, Preparation and properties of composite PAN/PANI membranes, Int. J. Polym. Sci., 2017 (2017) 1–14.
[27] J. Ren, J.R. McCutcheon, Polyacrylonitrile supported thin film composite hollow fiber membranes for forward osmosis, Desalination, 372 (2015) 67–74.
[28] R.S. Porter, Development of high ductility and tensile properties by a two-stage draw of poly(acrylonitrile): effect of molecular weight, J. Polym. Sci., Part B: Polym. Phys., 36 (1997) 629–640.
[29] M. Sniechowski, R. Borek, K. Piwowarczyk, W. Luzny, New structural model of PANI/CSA conducting polymer system obtained by molecular dynamics simulations, Macromol. Theory Simul., 24 (2015) 284–290.
[30] X. Guo, G.T. Fei, H. Su, L. De Zhang, High-performance and reproducible polyaniline nanowire/tubes for removal of Cr(VI) in aqueous solution, J. Phys. Chem. C, 115 (2011) 1608–1613.
[31] B.T. Raut, M.A. Chougule, S.R. Nalage, D.S. Dalavi, S. Mali, P.S. Patil, V.B. Patil, CSA doped polyaniline/CdS organic-inorganic nanohybrid: physical and gas sensing properties, Ceram. Int., 38 (2012) 5501–5506.
[32] G.D. Khuspe, S.T. Navale, M.A. Chougule, V.B. Patil, Ammonia gas sensing properties of CSA doped PANi-$SnO_2$ nanohybrid thin films, Synth. Met., 185 (2013) 1–8.
[33] J.A. Marins, B.G. Soares, K. Dahmouche, S.J.L. Ribeiro, H. Barud, D. Bonemer, Structure and properties of conducting bacterial cellulose-polyaniline nanocomposites, Cellulose, 18 (2011) 1285–1294.
[34] Z. Bashir, Polyacrylonitrile, an unusual linear homopolymer with two glass transitions, Indian J. Fibre Text. Res., 24 (1999) 1–9.
[35] Z. Bashir, The hexagonal mesophase in atactic polyacrylonitrile: a new interpretation of the phase transitions in the polymer, J. Macromol. Sci., Phys., 40 (2001) 41–67.
[36] Z. Bashir, S.P. Church, D. Waldron, Interaction of water and hydrated crystallization in water-plasticized polyacrylonitrile films, Polymer, 35 (1994) 967–976.
[37] A. Al-Ahmed, F. Mohammad, M.Z.A. Rahman, Preparation, characterization, thermooxidative degradation, and stability of polyaniline/polyacrylonitrile composites in terms of direct-current electrical conductivity retention, J. Appl. Polym. Sci., 99 (2006) 437–448.
[38] V. Kumar, T. Yokozeki, T. Goto, T. Takahashi, Synthesis and characterization of PANI-DBSA/DVB composite using roll-milled PANI-DBSA complex, Polymer, 86 (2016) 129–137.
[39] G. Zhai, Q. Fan, Y. Tang, Y. Zhang, D. Pan, Z. Qin, Conductive composite films composed of polyaniline thin layers on microporous polyacrylonitrile surfaces, Thin Solid Films, 519 (2010) 169–173.
[40] S. Zhao, Z. Wang, X. Wei, X. Tian, J. Wang, S. Yang, S. Wang, Comparison study of the effect of PVP and PANI nanofibers additives on membrane formation mechanism, structure and performance, J. Membr. Sci., 385–386 (2011) 110–122.

[41] B. Fryczkowska, L. Przywara, T. Turek, Application of PAN/PANI composite membranes in purification of industrial wastewater generated during processing of metals, Inżynieria Ekol., 18 (2017) 21–29.
[42] J. Ren, X. Huang, N. Wang, K. Lu, X. Zhang, W. Li, D. Liu, Preparation of polyaniline-coated polyacrylonitrile fiber mats and their application to Cr(VI) removal, Synth. Met., 222 (2016) 255–266.
[43] M.J. Corbatón-Báguena, S. Álvarez-Blanco, M.C. Vincent-Vela, Cleaning of ultrafiltration membranes fouled with BSA by means of saline solutions, Sep. Purif. Technol., 125 (2014) 1–10.
[44] Y.N. Wang, C.Y. Tang, Protein fouling of nanofiltration, reverse osmosis, and ultrafiltration membranes—the role of hydrodynamic conditions, solution chemistry, and membrane properties, J. Membr. Sci., 376 (2011) 275–282.
[45] L. Hou, Z. Wang, P. Song, A precise combined complete blocking and cake filtration model for describing the flux variation in membrane filtration process with BSA solution, J. Membr. Sci., 542 (2017) 186–194.
[46] M. Hashino, K. Hirami, T. Ishigami, Y. Ohmukai, T. Maruyama, N. Kubota, H. Matsuyama, Effect of kinds of membrane materials on membrane fouling with BSA, J. Membr. Sci., 384 (2011) 157–165.